Organic Electronics 15 (2014) 1306–1311

Contents lists available at ScienceDirect

Organic Electronics

journal homepage: www.elsevier.com/locate/orgel

Enhanced absorbance and electron collection in inverted organic solar cells: Optical admittance and transient photocurrent analyses

Zhiming Kam [a,b,1], Qingyi Yang [c,1], Xizu Wang [b], Bo Wu [c], Furong Zhu [c,*], Jie Zhang [b], Jishan Wu [a,b,*]

[a] Department of Chemistry, National University of Singapore, 3 Science Drive, Singapore 117543, Singapore
[b] Institute of Materials Research and Engineering, 3 Research Link, Singapore 117602, Singapore
[c] Department of Physics and Institute of Advanced Materials, Hong Kong Baptist University, Hong Kong

ARTICLE INFO

Article history:
Received 8 February 2014
Received in revised form 21 March 2014
Accepted 21 March 2014
Available online 4 April 2014

Keywords:
Organic solar cells
Lifetime
Optical admittance analysis
Transient photocurrent

ABSTRACT

Optical admittance analysis reveals that light absorption in inverted organic solar cells (OSCs), based on the same polymer blend layer of regio-regular poly(3-hexylthiophene):[6,6]-phenyl-C61-butyric acid methyl ester (PCBM), is always greater than their regular geometry OSCs fabricated using an ITO/poly(3,4-ethylene dioxythiophene):(polystyrene sulfuric acid) anode. Transient photocurrent measurements elucidate that interfacial exciton dissociation at the cathode interfaces of Al-modified ITO/PCBM (inverted cell) and Al/PCBM (regular cell) is not equivalent. It is shown that the reverse configuration allows improving the absorbance of the cell, favoring charge collection at cathode/PCBM interface and also possessing a dawdling degradation behavior as compared to a control regular OSC in the accelerated aging test.

1. Introduction

Organic solar cells (OSCs) are a promising alternative photovoltaic technology to conventional inorganic solar cells due to their low cost solution process fabrication capability. A broad range of distinct device technologies based on organic small molecules and polymeric photoactive materials are being developed very rapidly. Power conversion efficiency (PCE) of >9.2% [1] for single junction OSCs and ~10% for tandem OSCs have been demonstrated recently [2]. Apart from the encouraging results in achieving high PCE for OSCs, realizing stabile OSC performance over a long operation lifetime also attracts a significant research effort. The commonly used bulk heterojunction (BHJ) OSCs, forming so called regular OSC structure, have a donor/acceptor blend sandwiched between a front transparent indium tin oxide (ITO) anode and a reflective rear metal cathode. In regular OSCs, a hole-transporting buffer layer of poly(3,4-ethylene dioxythiophene):(polystyrene sulfuric acid) (PEDOT:PSS) is often deposited on ITO surface to assist in hole transport and hole extraction at the ITO/organic interface. It has been shown that the use of acidic PEDOT:PSS hole-transporting layer is not the best choice for efficient operation of OSCs over a long period of time, due to the deterioration in the contact property at ITO/PEDOT:PSS interface [3]. The upper metallic cathode in regular OSCs often undergoes a gradual oxidation resulting in a thermally unstable cathode/organic interface [4].

* Corresponding authors. Address: Department of Physics, Hong Kong Baptist University, 224 Waterloo Road, Kowloon Tong, Hong Kong. Tel.: +852 34115867; fax: +852 34115813 (F.R. Zhu), Department of Chemistry, National University of Singapore, 3 Science Drive, Singapore 117543, Singapore (J. Wu).
E-mail addresses: frzhu@hkbu.edu.hk (F. Zhu), chmwuj@nus.edu.sg (J. Wu).
[1] These authors contributed equally to this work.

http://dx.doi.org/10.1016/j.orgel.2014.03.032
1566-1199/

A comprehensive study on the degradation mechanisms of the regular structured OSC, based on the blend of regioregular poly(3-hexylthiophene) (P3HT):[6,6]-phenyl-C61-butyric acid methyl ester (PCBM) system, has been performed. The unbalanced charge mobility in the photoactive layer, due to oxygen-induced charge traps, is one of the degradation mechanisms [5]. In a previous work, we identified two distinguishable degradation pathways in the regular OSC [6]. One is associated with a localized failure related to the moisture encroachment in the charge generation area, inducing the charge recombination and thus eliminating the photocurrent. The other is dominated by an inevitable initial oxidation at the organic/cathode interface due to the presence of residual moisture and oxygen, leading to lowering PCE of OSCs. The degradation caused by the interfacial passivation could be avoided by the removal of the low work function cathode. This implies that the reverse configuration with a relatively environmental sensitive cathode/organic interface away from the top contact in the cell is preferred compared to the regular OSC.

Inverted OSCs, having an organic functional photoactive layer sandwiched between a front transparent cathode and a rear anode, are preferable for efficient cell operation. In this device configuration, a PEDOT:PSS hole transporting layer is not existent, avoiding the use of acidic PEDOT:PSS on ITO surface. In inverted OSCs, ITO surface is modified with a suitable low work function interlayer serving as a transparent cathode, for example, solution-processable ZnO [7], TiO_2 [8] and Cs_2CO_3 [9], low work function metals of Ca [10] and Al [11], and surface dipole-inducing materials [12]. However, the optical advantages, interfacial exciton dissociation at the cathode/organic interface and operational stability of the inverted OSCs have not yet been studied systemically. In this work, we show that the reverse configuration allows improving the absorbance of the cell, therefore its PCE. Transient photocurrent measurements indicate that interfacial exciton dissociation at the cathode/organic interfaces of Al-modified ITO/PCBM (inverted cell) and PCBM/Al (regular cell) is not equivalent. PCBM on Al-modified ITO forms a more abrupt interface than the energetic Al deposited on PCBM. X-ray Photoelectron Spectroscopy (XPS) analyses suggest that an ultrathin Al on ITO is partially oxidized, resulting in a reduction in ITO surface work function and acting as an effective transparent cathode. The operation stability of inverted OSCs, fabricated with a pair of an ultrathin Al-modified ITO front cathode and a MoO_3/Ag anode, was demonstrated by accelerated aging test in air.

2. Experimental

OSCs reported in this work were fabricated on ITO/glass substrates with a sheet resistance of ~15 Ω/square. The ITO substrates were pre-cleaned by ultrasonication in detergent solution, de-ionized water, acetone and isopropanol for 10 min sequentially. For the inverted OSCs, the surface of ITO/glass substrates was modified with ~1.2 nm thick Al, deposited by thermal evaporation in vacuum with a base pressure of $<1.0 \times 10^{-4}$ Pa at an evaporation rate of 0.1 Å/s. The ITO/glass substrates were not subjected to the oxygen plasma treatment before or after the surface modification enabling a simpler OSC fabrication process. The Al-modified ITO substrates were then transferred to an adjacent glove box with O_2 and H_2O levels below 1.0 ppm, which is connected to the evaporator. A pre-prepared polymer blend of P3HT (Rieke Metals) and PCBM (Nano-C), dissolved separately in 1,2-dichlorobenzene solution in a weight ratio of 1:0.8, was spin-coated on ultrathin Al-modified ITO front transparent cathode. The resulting inverted OSCs have a structure of ITO/Al (~1.2 nm)/P3HT:PCBM (200 nm)/MoO_3 (5 nm)/Ag (100 nm) and an active area of 3.0 mm × 3.0 mm. A control regular OSC with a structure of ITO/PEDOT:PSS (40 nm), Clevios P VP AI 4083/P3HT:PCBM (200 nm)/Al (100 nm) was also made for comparison study. Current density–voltage (J–V) characteristics of OSCs were measured under AM1.5G illumination at 100 mW/cm^2 (SAN-EI Electric XEC-301S solar simulator). Light intensity of the solar simulator was calibrated using a monosilicon detector (with KG-5 visible color filter) to minimize the spectral mismatch. After the control and the inverted OSCs were fabricated, they were kept inside N_2-purged glove box to stabilize for 3 days prior to the cell encapsulation. The encapsulated OSCs were then removed from the glove box for aging test in air. The accelerated lifetime measurements were carried out by continuous light soaking using a calibrated AM1.5G solar simulator, with light intensity of 100 mW/cm^2 under open-circuit condition at 60 ± 5 °C.

3. Results and discussion

J–V characteristics of the inverted and control regular OSCs are plotted in Fig. 1(a), insets in Fig. 1(a) are the cross-sectional views of the inverted OSC and control regular cell. It is shown that the open-circuit voltage (V_{OC}), short-circuit current density (J_{SC}) and fill factor (FF) of the inverted OSC increased from 0.59 V to 0.60 V, 9.98 mA/cm^2 to 10.30 mA/cm^2 and 0.63 to 0.68, respectively, making up for an overall 13% increase in PCE from 3.67% to 4.16%. The enhancement in PCE of the inverted OSC comes primary from a steady improvement in J_{SC} and FF, as can be seen in Fig. 1(a). This suggests that light absorption and photo-generated carrier transporting are more favorable in the reverse configuration of the cell, although the same photoactive layer thickness was used in both types of the cells. In P3HT:PCBM-based BHJ OSCs, an undesirable PCBM-rich blend layer appeared at the anode/organic interface, formed by the segregation of fullerene from the P3HT:PCBM blend due to its relatively poorer solubility in the organic solvent [13]. The presence of a PCBM-rich region at the PEDOT:PSS/P3HT:PCBM interface induces an adverse interfacial barrier for hole extraction in regular OSCs. In the reverse configuration, the removal of the interfacial barrier at the Al-modified ITO/PCBM-rich interface favors the electron collection, as compared to the hole collection at the PEDOT:PSS/PCBM-rich interface in the regular OSC. This can be seen by a reduced series resistance (R_S) in the cell, e.g., from 8.7 Ω for a control regular OSC to 7.1 Ω for an inverted OSC.

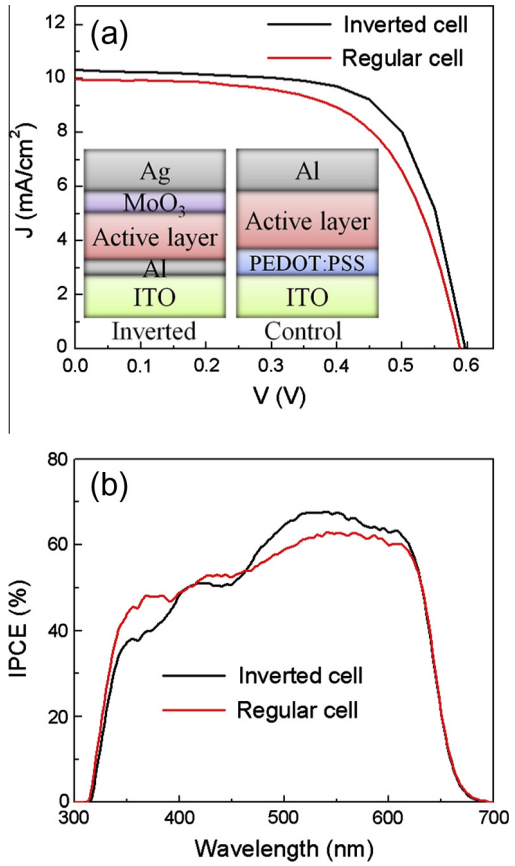

Fig. 1. (a) *J–V* characteristics measured for an inverted OSC of ITO/Al (~1.2 nm)/P3HT:PCBM (200 nm)/MoO_3 (5 nm)/Ag (100 nm) (black solid line), and a control regular OSC of ITO/PEDOT:PSS (40 nm)/P3HT:PCBM (200 nm)/Al (100 nm) (red solid line). Insets in Fig. 1(a): the cross-sectional views of the inverted and control regular OSCs. (b) A comparison of the corresponding IPCE spectra measured for the inverted and control regular cells. (For interpretation of the references to colour in this figure legend, the reader is referred to the web version of this article.)

Incident photon to current efficiency (IPCE) characteristics of the inverted OSC and a control regular cell were also measured and are shown in Fig. 1(b). IPCE characteristics provide the information of light absorption in the active region contributing to exciton generation and average external quantum efficiency of the OSCs. Although the same thickness of actual photoactive layers in the inverted and the control cells was used, absorption enhancement in the active layer is dependent on the cell design and architecture. The change in the IPCE spectra at wavelength <400 nm and the region from 450 nm to 600 nm, as depicted in Fig. 1(b), is attributed to the interference effect. It is advantageous to optimize optical field distribution in the wavelength region corresponding to the maximal absorption of the blend, thereby improving exciton generation in OSCs. An obvious increase in IPCE over the wavelength range from 450 nm to 600 nm, corresponding to the maximum absorption profile of the P3HT:PCBM blend layer, is clearly observed in the inverted OSC as compared to a control regular cell. J_{SC} calculated using IPCE spectra of the inverted OSC and a control regular cell also agrees with measured *J–V* characteristics, showing that the improvement in PCE of the inverted OSC is attributed to the improvement in J_{SC} and *FF*. A summary of device parameters obtained for the inverted and control regular cells is listed in Table 1.

With the intention of better understanding the difference in the performance of the reverse configuration and regular OSCs, the absorbance of both types of the cells was examined using optical admittance analysis. From optical point view, an OSC can be considered as a thin film system composed of absorbing and non-absorbing materials, as depicted in the cross-sectional views of the BHJ OSCs in insets of Fig. 1(a). The optical properties of an OSC can be optimized to realize maximal light absorption in the organic photoactive layer. Defining $F(\lambda)$ as the flux of the sun light incident on an OSC, e.g., AM1.5G spectrum used in the simulation, the integrated absorptance of the photoactive layer, $\overline{A}$, can be calculated using the following equation [14,15]:

$$\overline{A} = \frac{\int A(\lambda)F(\lambda)d\lambda}{\int F(\lambda)d\lambda} \quad (1)$$

where $A(\lambda)$ is the spectral absorbance of the organic photoactive layer. The wavelength dependent refractive indices of each layer in the OSC system were measured using variable angle spectroscopic ellipsometry. It becomes possible to optimize the thickness of organic photoactive layer (e.g., P3HT:PCBM) through maximizing its integrated absorptance.

The integrated absorptance of the organic photoactive layer, calculated for the inverted and control regular OSC as a function of the P3HT:PCBM layer thickness from 0 to 300 nm, is shown in Fig. 2. For both types of OSCs having the same active layer thickness, it is evident that the reverse configuration allows improving the absorbance of the cell and therefore its PCE. $\overline{A}$ shows an oscillation behavior with increase in the thickness of P3HT:PCBM blend layer in both types of OSCs. There are two relative absorption maxima occurred at the blend layer thicknesses of ~70 nm and 200 nm for the inverted OSC, and ~75 nm and 225 nm for the control regular cell, which correspond to a relatively higher photocurrent generation in OSCs. In Fig. 2, it is clear that a 200 nm thick P3HT:PCBM layer, taken as the optimal thickness for the inverted OSC, apparently absorbs more light than the control regular OSC having a 225 nm thick photoactive layer. It is known that light absorption in OSCs is limited due to the presence of a mismatch between optical absorption length and charge transport scale, caused by the low charge mobility in conjugated polymers. Thus a thinner photoactive layer used in the inverted OSC with improved light absorbance, as shown in Fig. 2, is preferred to reduce the exciton recombination losses and also to increase drift velocity of the carrier in higher electric field. The above discussion based on optical admittance analysis agrees with the experimental results in showing that the inverted OSCs having a 200 nm thick P3HT:PCBM layer corresponded to the best cell performance, as presented in Fig. 1.

Table 1
Device performance of the inverted and control regular OSCs measured at AM1.5G of 100 mW/cm^2, the values of J_{SC} and PCE calibrated using IPCE measurements are also given in the parentheses for comparison.

	Cell configuration	V_{OC} (V)	J_{SC} (mA/cm^2)	*FF*	PCE (%)	R_S (Ω)
(a)	Inverted OSC	0.60	10.30 (9.72)	0.68	4.16 (3.93)	7.1
(b)	Control regular OSC	0.59	9.98 (9.43)	0.63	3.67 (3.47)	8.7

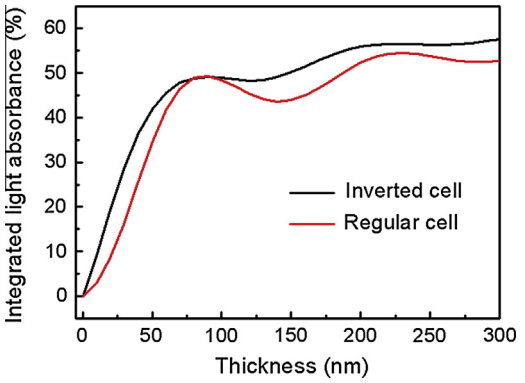

Fig. 2. A comparison of integrated absorbance of P3HT:PCBM photoactive layer as a function of its thickness, calculated for an inverted OSC and a control regular cell over the P3HT:PCBM thickness range from 0 to 300 nm.

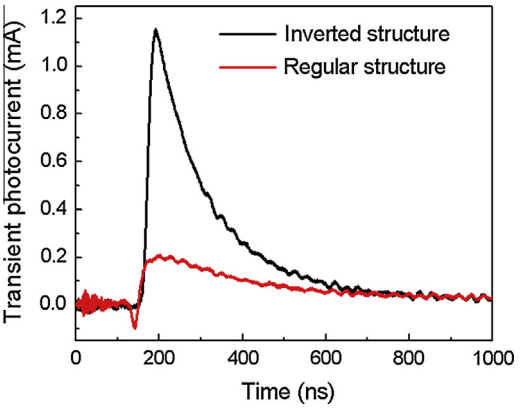

Fig. 3. Transient photocurrent measured for an ITO/Al(10 nm)/PCBM(400 nm)/MoO_x/Ag device, compared to that of a control ITO/PEDOT:PSS/PCBM(400 nm)/Al(30 nm) sample, at a forward bias of 0.4 V. The transient photocurrent measured using a small optical perturbation from cathode sides of ITO/Al(10 nm)/PCBM(400 nm) and Al(30 nm)/PCBM(400 nm) of the inverted and regular devices.

The combination of ultrathin metals and transparent conducting oxide (TCO) for application in OSCs has been reported [16,17]. It was found that the insertion of an ultrathin metal film between the TCO and the organic layer improves the cell performance due to a batter carrier collection and energy level matching. In order to examine the interfacial exciton dissociation at the cathode interfaces of Al-modified ITO/PCBM-rich (inverted cell) and PCBM/Al (regular cell), a 400 nm thick PCBM layer was used in the reverse and regular structured devices for transient photocurrent (TPC) measurements, e.g., ITO/Al(10 nm)/PCBM(400 nm)/MoO_x/Ag and ITO/PEDOT:PSS/PCBM(400 nm)/Al(30 nm). This allows analyzing the interfacial exciton dissociation at the organic/cathode interface in the absence of internal built-in potential [18]. For the TPC measurement, transient photocurrent was recorded using a small optical perturbation from cathode sides of ITO/Al(10 nm)/PCBM(400 nm) and Al(30 nm)/PCBM(400 nm) of the inverted and regular devices, illuminated using a pulsed Nd:YAG laser with the wavelength of 355 nm and pulse duration of <5 ns at a forward bias of 0.4 V.

Transient photocurrent results are shown in Fig. 3. It is observed that decays in transient photocurrent of the regular and inverted devices exhibit different behavior. The transient photocurrent, measured for the ITO/PEDOT:PSS/PCBM(400 nm)/Al(30 nm) device, replicated the interfacial exciton dissociation at the PCBM/Al contact of the regular device. It is clear that there is a polarity change from negative to positive in the transient photocurrent. The prompt negative transient photocurrent flow, which originates from the fast interfacial exciton dissociation at the PCBM/Al interface, is apparently disadvantageous for the electron collection. However there was no measurable negative transient photocurrent for the ITO/Al(10 nm)/PCBM(400 nm)/MoO_x/Ag in the TPC measurement. This suggests that the interfacial exciton dissociation at cathode interface of the inverted cell generated an alike transient photocurrent flow that is favorable for the electron collection. The asymmetrical behavior is essentially originated from the difference of the contact properties, depending on the sequence of forming an organic layer on Al contact or depositing Al cathode on organic layer. When an organic layer is coated on Al by the solution-processed approach, the strongly bonded metal surface atoms are not affected and a relatively clear Al/PCBM interface in the inverted structure is expected. However, the relatively weak van der Waals interaction between molecules in the organic layer can be easily disturbed by the deposition of energetic metal atoms, typically evaporated at elevated temperatures. The penetration of energetic Al atoms into the underlying functional organic layer is primary responsible for the complex PCBM/Al interfacial properties in the regular structure. Transient photocurrent measurements indicate clearly that interfacial exciton dissociation at cathode interfaces of Al-modified ITO/PCBM (inverted cell) and PCBM/Al (regular cell) is not equivalent. It is expected that PCBM on Al-modified ITO forms a more abrupt interface than the energetic Al deposited on PCBM, leading to an asymmetric interfacial exciton dissociation behavior. It is

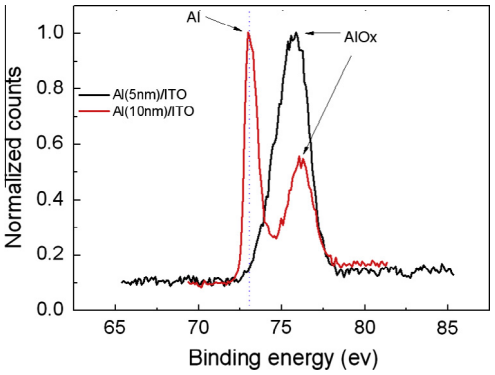

Fig. 4. XPS Al_{2p} peaks measured for the surfaces of ITO overlaid with 5 nm and 10 nm thick Al, revealing the chemical state of ultrathin Al on ITO. Oxidized Al was found on ITO surface when its coverage is <5 nm in vacuum.

shown that the interfacial exciton dissociation at the cathode of the inverted cell favors the efficient electron collection as compared to the regular cell.

The electronic properties of ultrathin Al-modified ITO interface were studied by XPS measurement. As shown in Fig. 4, for an ultrathin layer of Al on ITO surface, the XPS Al_{2p} peak with a higher binding energy of 75.8 eV can be observed, which corresponds to oxidized aluminum as compared to its metal Al state having a binding energy of XPS Al_{2p} peak at 73 eV. It shows that the first few nanometer thick Al reacts with the ITO resulting in the formation of a thin AlO_x layer on ITO surface. As the Al increased to ~10 nm, a dual Al_{2p} XPS peak with an additional peak at a binding energy at 73 eV, corresponding to metallic Al, started to form on ITO surface, suggesting the interface contained a mixture of Al and AlO_x. A reduction in work function of ITO was observed when the ITO surface was modified with an ultrathin Al layer, enabling the Al-modified ITO to serve as an efficient transparent cathode. This is confirmed by an increase in V_{OC} of inverted OSCs, as shown in Fig. 1(a). A reduction in work function of an ultrathin Al-modified ITO consists with the XPS measurements suggesting that an ultrathin AlO_x layer is formed on ITO. A thin AlO_x has a low work function as compared to ITO, as it is so thin it does not affect visible-light transparency of the front ITO cathode. The fullerene-rich P3HT:PCBM/AlO_x-ITO interface in the inverted OSCs is relatively stable and electrically favorable for electron extraction, resulting in more stability and efficient cell operation as compared to the normal OSCs.

The accelerated aging experiments were conducted for inverted and control regular OSCs by continuous light soaking in air. In order to establish a comprehensive and reliable OSC lifetime data for durability studies, the lifetime results are averaged from a set of inverted and control regular OSCs to establish the statistically reliable data. The normalized cell parameters of V_{OC}, *FF*, J_{SC} and PCE measured for the inverted and control cells as a function of aging time are shown in Fig. 5. The inverted OSCs experienced a much slower degradation in J_{SC} and *FF* as compared to the control regular OSCs. The results agree with the TPC measurements suggesting that the quality of the interfacial contacts in the reverse configuration of the cell function well for charge extraction during the aging, demonstrating the improved durability as compared to the control regular cell. Both types of the OSCs underwent an initial fast decrease in PCE, followed by an extended period of slower decay. The initial fast degradation for the inverted OSCs occurred within the first 10 h of aging, with a ~40% loss in PCE by the 70 h mark. Degradation of the inverted OSCs is much slower after passing the 70 h initial decay period under a continuous light soaking. However, the control regular OSCs experienced a faster decay in all cell parame-

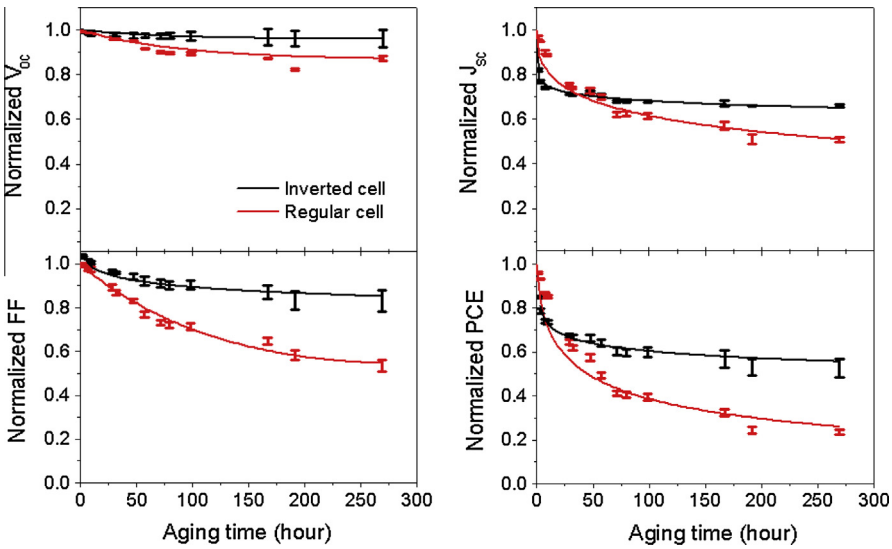

Fig. 5. J_{SC}, V_{OC}, *FF* and PCE versus aging time measured for the encapsulated inverted and regular OSCs under a continuous light soaking with light intensity of ~100 mW/cm^2 (AM1.5G) at 60 ± 5 °C in air.

ters in the first 70 h with ~60% loss in PCE, and a continuous degradation in PCE was observed as light soaking time increased.

4. Conclusions

The reverse configuration allows improving the absorbance of the cell, and therefore its PCE. Interfacial exciton dissociation at cathode interfaces of Al-modified ITO/PCBM and PCBM/Al is not equivalent. It is shown that Al-modified ITO/PCBM interface in the reverse configuration favors the efficient electron collection in the cell as compared to the regular device. High performance inverted P3HT:PCBM OSC with PCE of 4.16%, which is ~13% more efficient than the control regular cell (3.67%), was achieved using an ultrathin Al-modified ITO cathode and a bi-layer MoO_3/Ag anode. An improvement in operation stability of the inverted OSC was demonstrated using an accelerated aging test in air.

Acknowledgements

The work was supported by a grant from the Research Grants Council of the Hong Kong Special Administrative Region, China. Project No. T23-713/11, the National Natural Science Foundation of China (Grant No. 61275037) and Hong Kong Baptist University Faculty Research Grant (Project No. 30-12-252). J.W. acknowledges financial support from IMRE Core Funding (IMRE/13-1C0205) and MOE Tier 2 Grant (MOE2011-T2-2-130). J.Z. acknowledges the support from STAR SERC TSRP Grant (Project No. 102 170 0137).

References

[1] Z.C. He, C.M. Zhong, S.J. Su, M. Xu, H.B. Wu, Y. Cao, Nat. Photonics 6 (2012) 591.
[2] J.B. You, L.T. Dou, K. Yoshimura, T. Kato, K. Ohya, T. Moriarty, K. Emery, C.C. Chen, J. Gao, G. Li, Y. Yang, Nat. Commun. 4 (2013) 1446.
[3] M.P. deJong, L.J. van IJzendoorn, M.J.A. deVoigt, Appl. Phys. Lett. 77 (2000) 2255.
[4] M. Jørgensen, K. Norrman, F.C. Krebs, Sol. Energy Mater. Sol. Cells 92 (2008) 686.
[5] C. Vijila, G.M. Ng, Mein Jin Tan, W.P. Goh, F.R. Zhu, Appl. Phys. Lett. 95 (2009) 263305.
[6] X.Z. Wang, X.X. Zhao, G. Xu, Z.K. Chen, F.R. Zhu, Sol. Energy Mater. Sol. Cells 104 (2012) 1.
[7] H.X. Liu, Z.H. Wu, J.Q. Hu, Q.L. Song, B. Wu, H.L. Tam, Q.Y. Yang, W.H. Choi, F.R. Zhu, Appl. Phys. Lett. 103 (2013) 043309.
[8] S.K. Hau, H.L. Yip, H. Ma, A.K.Y. Jen, Appl. Phys. Lett. 93 (2008) 233304.
[9] H.H. Liao, L.M. Chen, Z. Xu, G. Li, Y. Yang, Appl. Phys. Lett. 92 (2008) 173303.
[10] C.Y. Jiang, X.W. Sun, D.W. Zhao, A.K.K. Kyaw, Y.N. Li, Sol. Energy Mater. Sol. Cells 94 (2010) 1618–1621.
[11] H.M. Zhang, J. Ouyang, Appl. Phys. Lett. 97 (2010) 063509.
[12] Y. Zhou, C. Fuentes-Hernandez, J. Shim, J. Meyer, A.J. Giordano, H. Li, P. Winget, T. Papadopoulus, H. Cheun, J. Kim, M. Fenoll, A. Dindar, W. Haske, E. Najafabadi, T.M. Khan, H. Sojoudi, S. Barlow, S. Graham, J.-L. Brédas, S.R. Marder, A. Kahn, B. Kippelan, Science 336 (2012) 327–332.
[13] M. Campoy-Quiles, T. Ferenczi, T. Agostinelli, P.G. Etchegoin, Y. Kim, T.D. Anthopoulos, P.N. Stavrinou, D.D.C. Bradley, J. Nelson, Nat. Mater. 7 (2008) 158.
[14] G.M. Ng, E.L. Kietzke, T. Kietzke, L.W. Tan, P.K. Liew, F.R. Zhu, Appl. Phys. Lett. 90 (2007) 103505.
[15] X.Z. Wang, G.M. Ng, J.W. Ho, H.L. Tam, F.R. Zhu, IEEE J. Sel. Top. Quant. Electron. 16 (2010) 1685.
[16] X.Z. Wang, J.W. Ho, Q.Y. Yang, H.L. Tam, G.X. Li, K.W. Cheah, F.R. Zhu, Org. Electron. 12 (2011) 1943.
[17] N. Formica, D.S. Ghosh, A. Martinez-Otero, T.L. Chen, J. Martorell, V. Pruneri, Appl. Phys. Lett. 103 (2013) 183304.
[18] Q.L. Song, H.R. Wu, X.M. Ding, X.Y. Hou, Appl. Phys. Lett. 88 (2006) 232101.